Electronic Supplementary Material (ESI) for Energy & Environmental Science.

Electronic Supplementary Information

Polymeric Room-Temperature Molten Salt as Multiple Functional Additive toward Highly Efficient and Stable Inverted Planar Perovskite Solar Cells

Shuangjie Wang,[a] Bowen Yang,[b] Jian Han,[a] Ziwei He,[a] Tongtong Li,[a] Qi Cao,[a] Jiabao Yang,[a] Jiajia Suo,[b] Xuanhua Li,[a]* Zhike Liu,[c] Shengzhong (Frank) Liu,[c] Chao Tang,[d] and Anders Hagfeldt[b]*

Affiliations:

a. State key Laboratory of Solidification Processing, Center for Nano Energy Materials, School of Materials Science and Engineering, Northwestern Polytechnical University, Xi´an 710072, China

b. Laboratory of Photomolecular Science, Institute of Chemical Sciences and Engineering, École Polytechnique Fédérale de Lausanne, Lausanne 1015, Switzerland.

c. School of Materials Science and Engineering, Shaanxi Normal University, Xi'an, 710119, China.

d. Key Laboratory for Organic Electronics & Information Displays (KLOEID), Institute of Advanced Materials. Nanjing University of Posts & Telecommunications. 9 Wenyuan Road, Nanjing 210023, China

* E-mail: lixh32@nwpu.edu.cn, anders.hagfeldt@epfl.ch

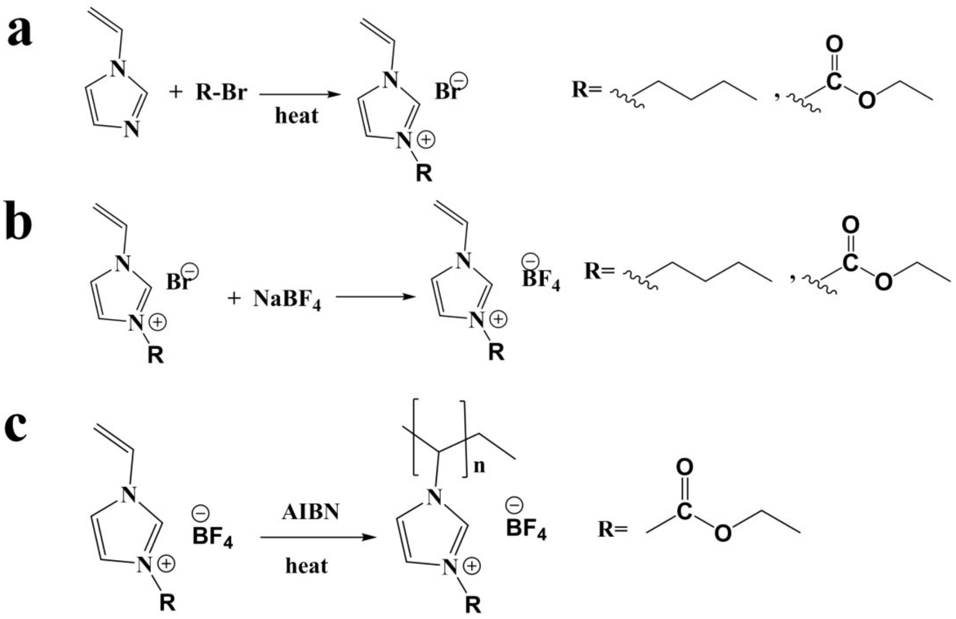

Fig. S1 The synthetic process of the Bu, Ea RTMS and PEa poly-RTMS.

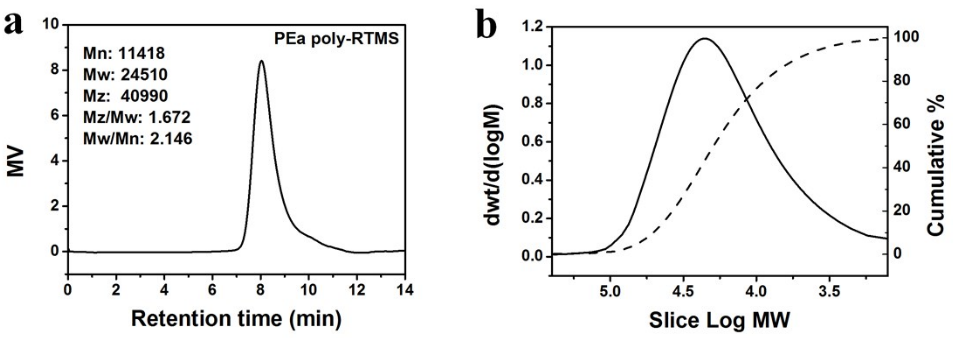

Fig. S2 (a) The gel permeation chromatography (GPC) curve and (b) molecular weight distribution of the PEa Poly-RTMS.

As shown in Fig. S2b, taking log Mw=4.0 (Mw=10000) as the median molecular weight, the proportion of log Mw>4.0 for PEa poly-RTMS reaches 76 %, while the proportion of log Mw<4.0 is only 24 %. The Mw/Mn represents polydispersity with a value of 2.146. For the free radical polymerization of vinyl, the molecular weight distribution of the product will be widened gradually when the reaction reaches the high conversion stage. Thus, the molecular weight distribution and polydispersity indicate that the PEa poly-RTMS has relative narrow molecular weight distribution.

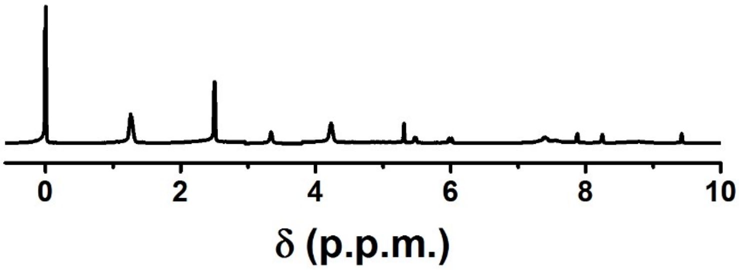

Fig. S3 ^{1}H NMR of the PEa poly-RTMS.

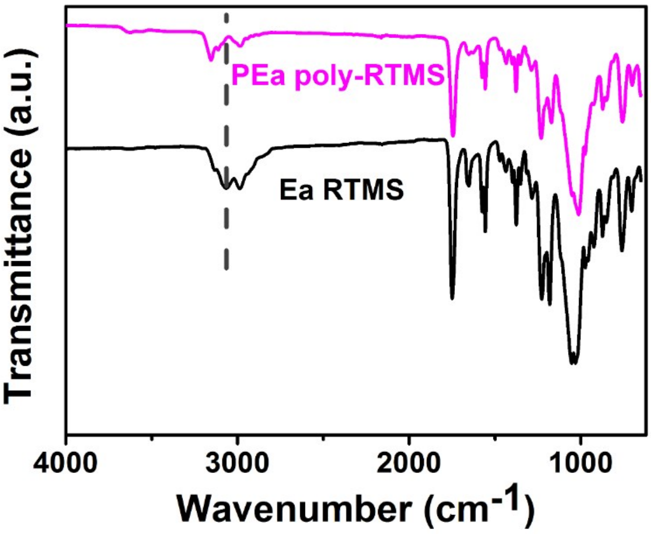

Fig. S4 FTIR spectra of the Ea RTMS and PEa poly-RTMS. Compared with the Ea RTMS, the disappearance of the vibration peak of -CH=CH_2 group (3070 cm^{-1}) in the PEa poly-RTMS indicates the high purity of the poly-RTMS.

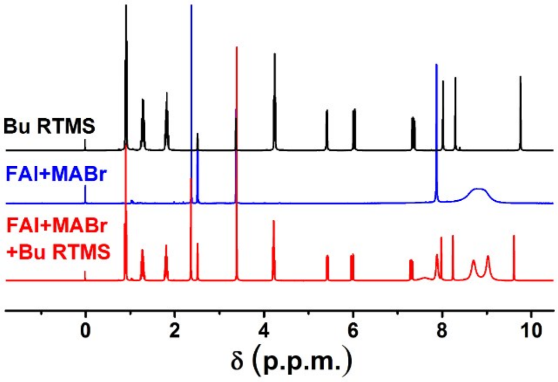

Fig. S5 ^{1}H NMR spectra of the Bu RTMS, FAI+MABr and FAI+MABr+Bu RTMS (Bu RTMS: 0.3 mg/ml) mixed solutions, respectively.

A broad peak around 9 ppm is correspond to the protons bound to nitrogen atoms in mixed solution of FAI and MABr, this peak splits into two new peaks due to interaction between the Bu RTMS and these protons upon addition of Bu RTMS. Considering the amount of FAI is larger than MABr in perovskite precursor solution, we speculated that this peak splitting might be related to the changes of the chemical environment of FA in the presence of Bu RTMS.

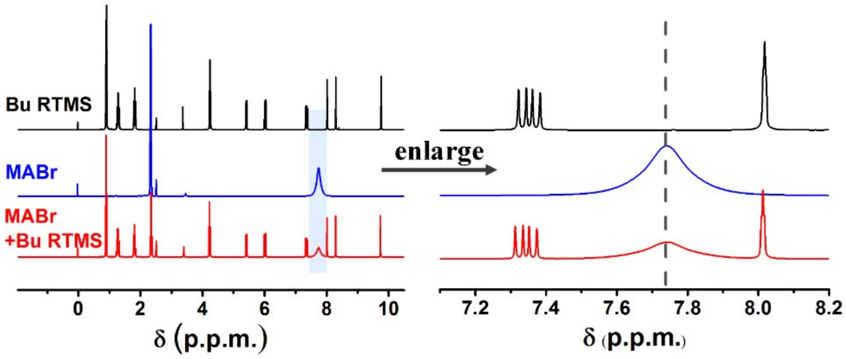

Fig. S6 ^{1}H NMR spectra of the Bu RTMS, MABr and MABr+Bu RTMS (0.3 mg/ml) mixed solutions.

To further ascertain the reaction, we conducted additional ^{1}H NMR spectrum of only MABr solution to which Bu RTMS was added and no clear peak shift and splitting were observed in Fig. S6. Comprehensive above results corroborate that the peak splitting is attributed to hydrogen bonds of the amidinium moiety in FA.

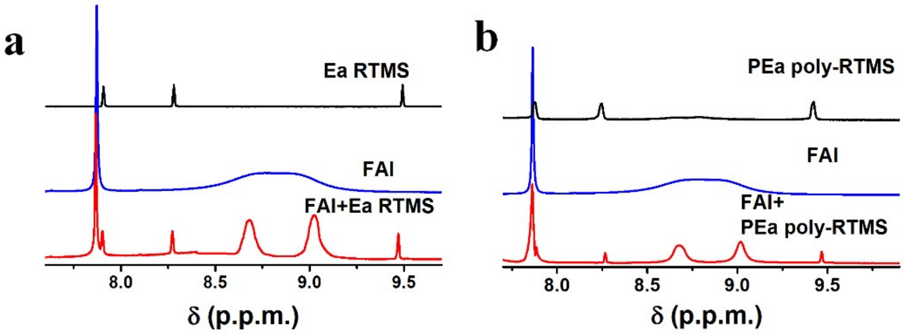

Fig. S7 ^{1}H NMR spectra of the a) Ea RTMS, FAI and FAI+Ea RTMS (Ea RTMS: 0.6 mg/ml) mixed solutions and b) PEa poly-RTMS, FAI and FAI+PEa poly-RTMS (PEa poly-RTMS: 0.13%) mixed solutions, respectively.

A broad peak around 9 ppm in the mixed solution is correspond to the protons bound to nitrogen atoms, which splits into two new peaks due to interaction between the Ea RTMS (or PEa poly-RTMS) and these protons of FAI. These results verify that the peak splitting is attributed to hydrogen bonds of the amidinium moiety in FA.

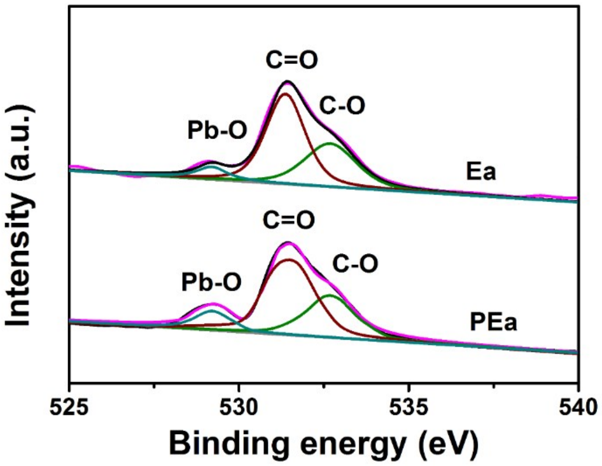

Fig. S8 XPS O 1s core level of the Ea- and PEa-modified perovskite films. The components of Pb-O, C=O and C-O locate at 529.4 eV, 531.5 eV and 532.8 eV, respectively.[1, 2]

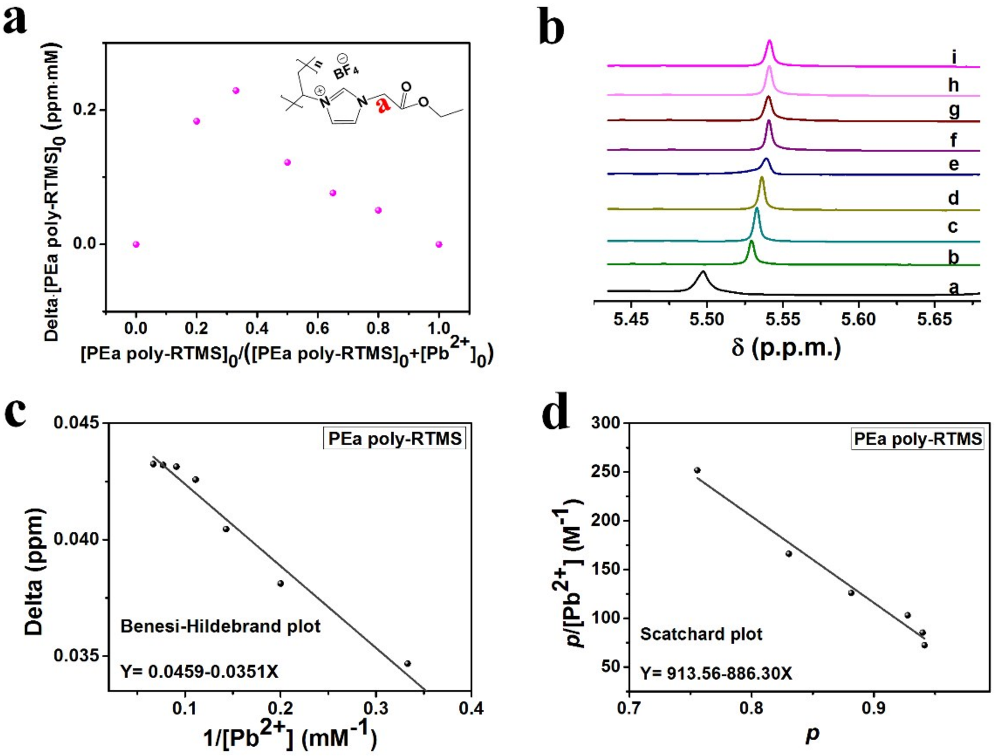

Fig. S9 a) Job plot. Stoichiometry of the complexation between PEa poly-RTMS and Pb^{2+} in DMSO-d6. Delta is chemical shift change of a-H. [PEa poly-RTMS]$_0$+[Pb^{2+}]$_0$=5 mM. [PEa poly-RTMS]0 and [Pb^{2+}]0 are the initial concentration of PEa poly-RTMS and Pb^{2+}. b) Partial ^{1}H NMR spectra of PEa poly-RTMS at the concentration of 1.5 mM with addition of Pb^{2+}: (a) 0 mM; (b) 1 mM; (c) 3 mM; (d) 5 mM; (e) 7 mM; (f) 9 mM; (g) 11 mM; (h) 13 mM; (i) 15 mM; c) Benesi-Hildebrand plot and d) Scatchard plot for the complexation of Pb^{2+} with PEa poly-RTMS.

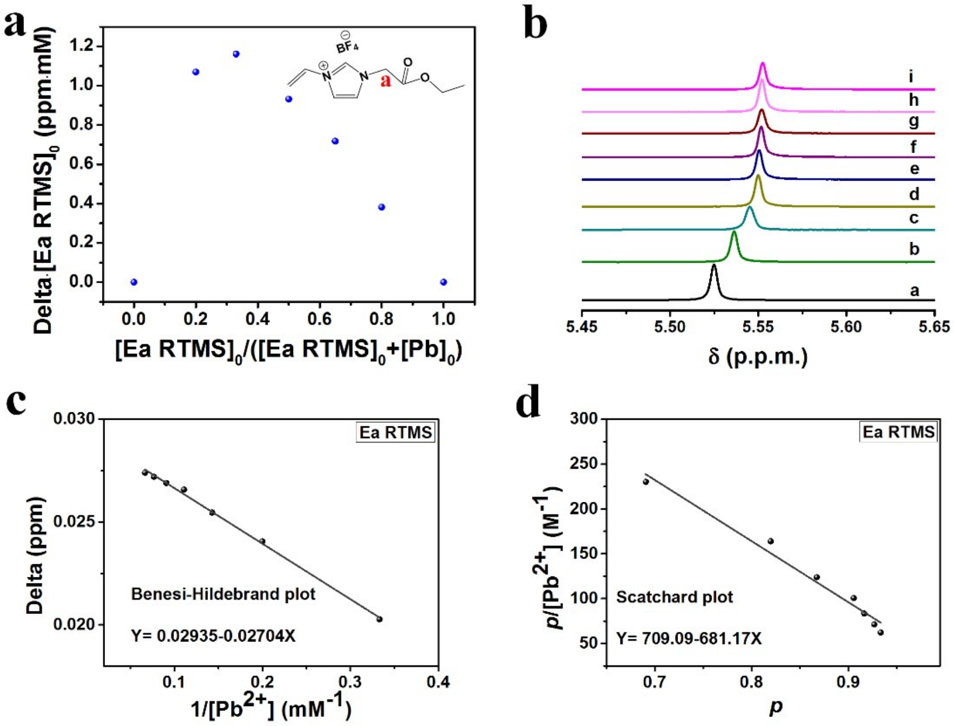

Fig. S10 a) Job plot. Stoichiometry of the complexation between Ea RTMS and Pb^{2+} in DMSO-d6. Delta is chemical shift change of a-H. $[\text{Ea RTMS}]_0+[\text{Pb2+}]_0=50$ mM. $[\text{Ea RTMS}]_0$ and $[Pb^{2+}]_0$ are the initial concentration of Ea RTMS and Pb^{2+}. b) Partial 1H NMR spectra of Ea RTMS at the concentration of 2.5 mM with addition of Pb^{2+}: (a) 0 mM; (b) 1 mM; (c) 3 mM; (d) 5 mM; (e) 7 mM; (f) 9 mM; (g) 11 mM; (h) 13 mM; (i) 15 mM; c) Benesi-Hildebrand plot and d) Scatchard plot for the complexation of Pb^{2+} with Ea RTMS.

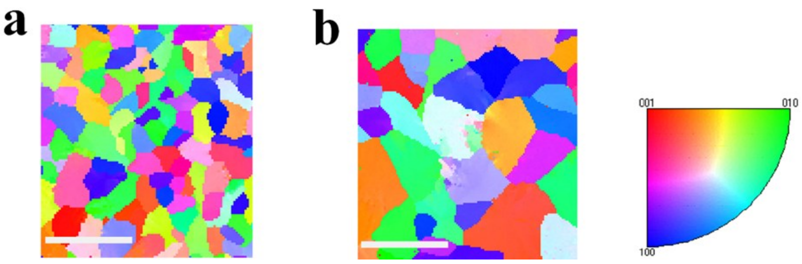

Fig. S11 Inverse pole images of (a) control and (b) PEa-modified perovskite films with individual back scatter diffraction patterns. The scale bar in images is 1 μm.

The PEa-modified perovskite film exhibits good crystallinity, and its grain size is larger than that of the control film, which are consistent with the observation in SEM measurement.

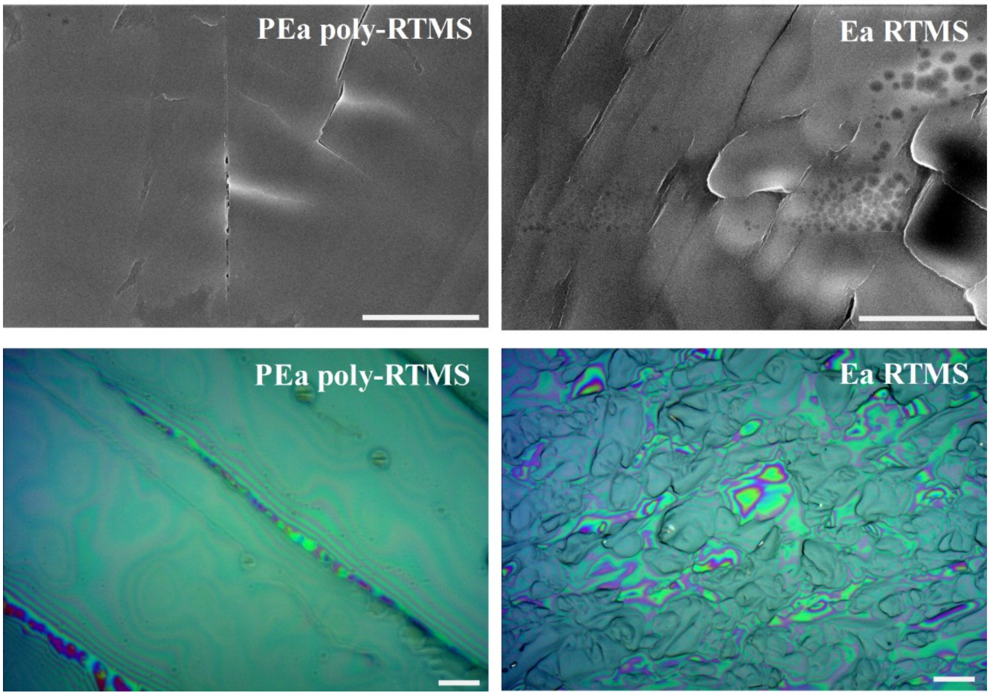

Fig. S12 Top-view SEM (scale bar: 5 μm) and optical microscopy images (scale bar: 20 μm) of PEa poly-RTMS and Ea RTMS deposited onto the ITO substrate.

The PEa poly-RTMS film shows good coverage and the Ea RTMS film exhibits obvious agglomeration, which indicate that the film-forming property of the PEa poly-RTMS is better than that of the Ea RTMS.

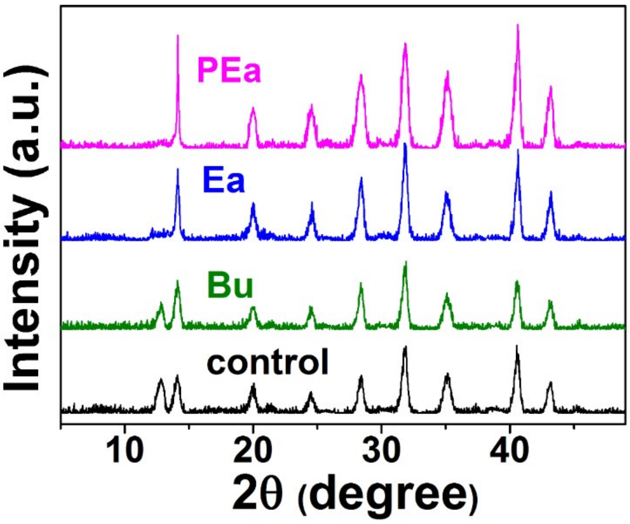

Fig. S13 XRD patterns of the control, Bu-, Ea- and PEa-modified perovskite films.

We conducted the XRD to further examine the effect of PEa poly-RTMS and RTMS monomers on the crystallization of perovskite films. No obvious peak shift or new peak are observed, indicating the large cations of PEa poly-RTMS and RTMS do not enter the perovskite lattice. A peak in control and Bu-modified films around 12.7° corresponding to the cubic phase of PbI_2,[3] while we found no impurity phases in the XRD for Ea- and PEa-modified films.

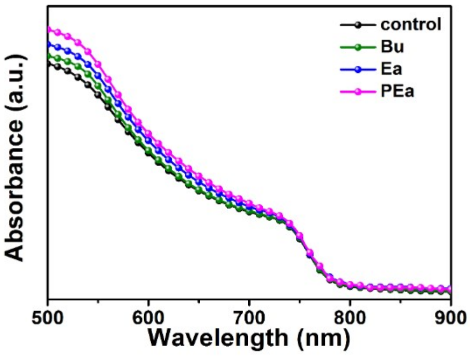

Fig. S14 UV–Vis absorption spectra of the control, Bu-, Ea- and PEa-modified perovskite films.

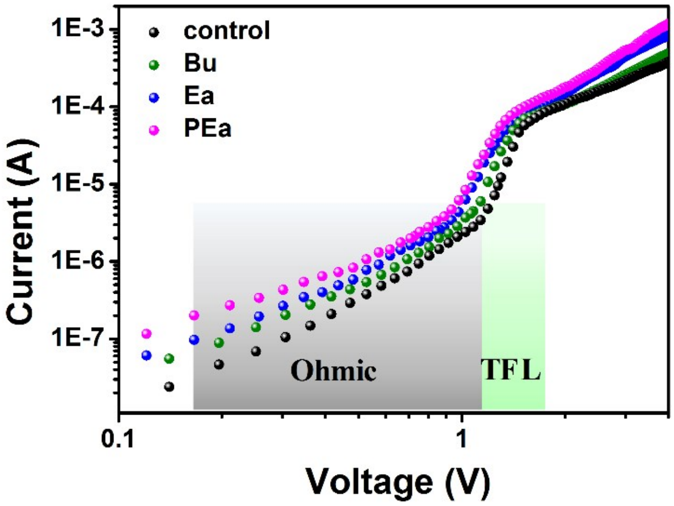

Fig. S15 Dark current-voltage response of hole-only devices, device structure: ITO/NiOx/perovskite/Spiro/Au.

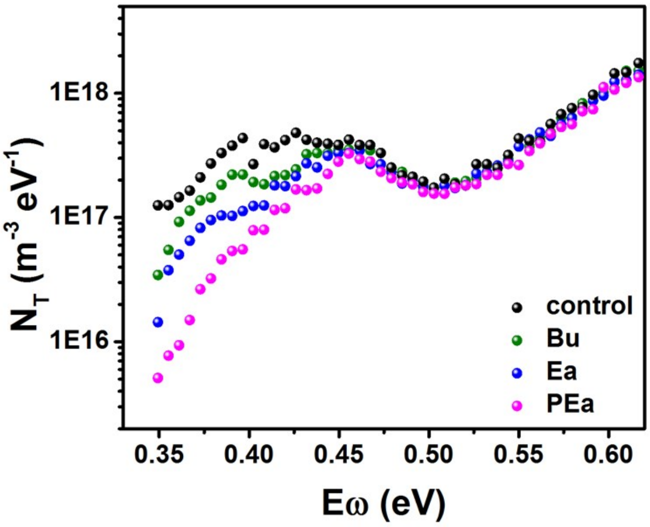

Fig. S16 The trap density of states (t-DOS) of control, Bu-, Ea-, and PEa-modified PSCs measured by TAS at 300 K.

The distribution in trap density of states can be derived from the equation: $N_T = -\frac{V_{bi}\,dC\ \ \omega}{qWd\omega k_B T}$, $E_\omega = k_B T ln\frac{\beta T^2}{\omega}$.[4] Where $V_{bi}$is the built-in potential, *W* is the depletion, *C* is the capacitance, *ω* is the angular frequency, *q* is the element charge, k_B is the Boltzmann's constant, and *T* is the temperature. The V_{bi} and *W* are obtained by Mott-Schottky plot though measuring the capacitance-voltage.

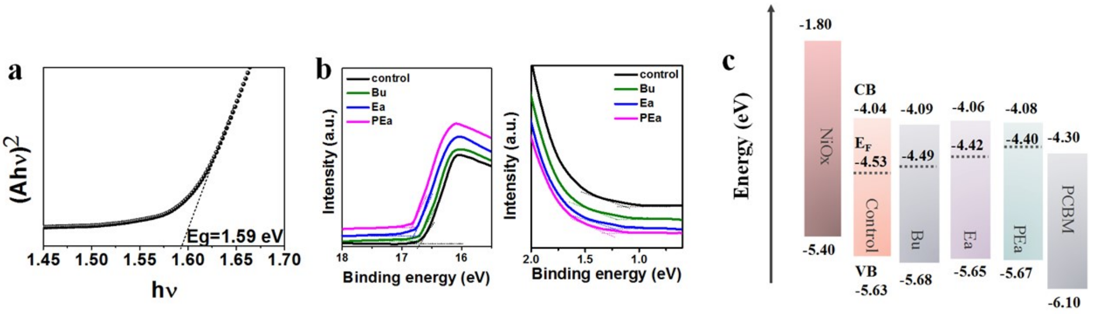

Fig. S17 (a) Tauc plots and (b) UPS characterization of the control, Bu-, Ea-, and PEa-modified films. (c) Energy band diagram of these different layers based on the parameters calculated from UPS spectra.

The bandgaps (Eg) derived from the UV–Vis absorption spectra of these modified films is 1.59 eV. The left panel (right) of the secondary-electron cut-off binding energies is 16.69 (1.10), 16.73 (1.19), 16.80 (1.23) and 16.82 (1.27) eV for control, Bu-, Ea-, and PEa-modified films, respectively. The E_F was obtained by $21.22 - E_{left\,panel}$. The VB was obtained by E_F- $E_{right\,panel}$. The position of the CB with respect to the VB was defined by the optical bandgap (1.59 eV). The VB and CB of modified films exhibit similar to the control film, as shown in Fig. S17. The Fermi level (E_F) of the modified films have slightly shifted to CB, which is beneficial to the charge transfer from perovskite film to electron transport layer.

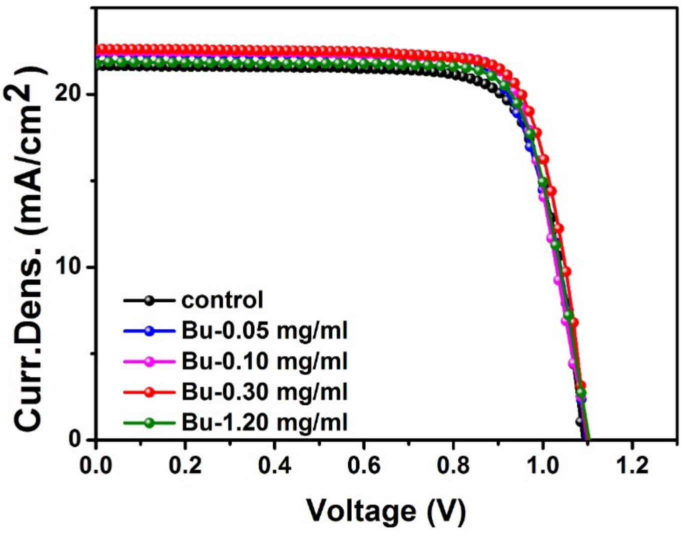

Fig. S18 *J-V* characteristic of the Bu-modified PSCs with different concentration of the Bu RTMS.

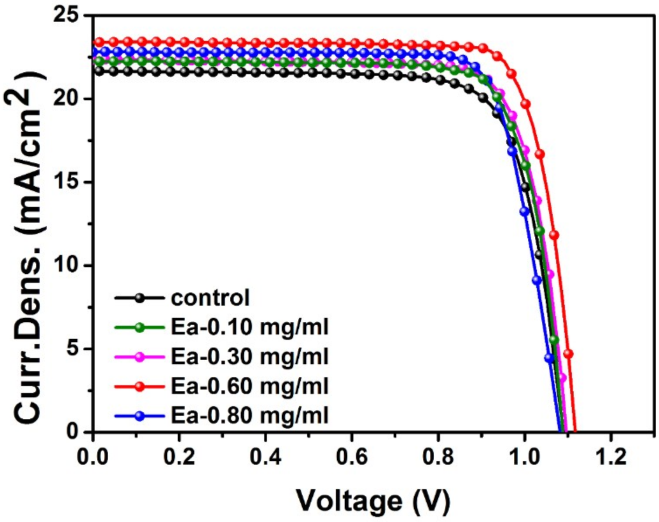

Fig. S19 *J-V* characteristic of the Ea-modified PSCs with different concentration of Ea RTMS.

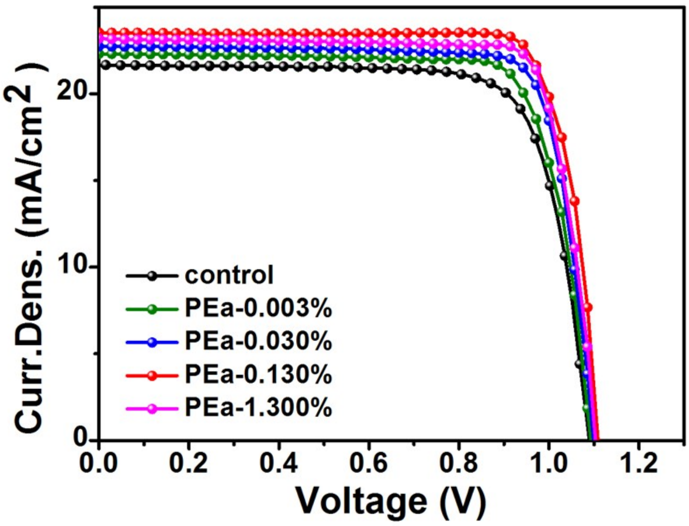

Fig. S20 *J*-*V* characteristic of PEa-modified PSCs with different concentration of PEa poly-RTMS.

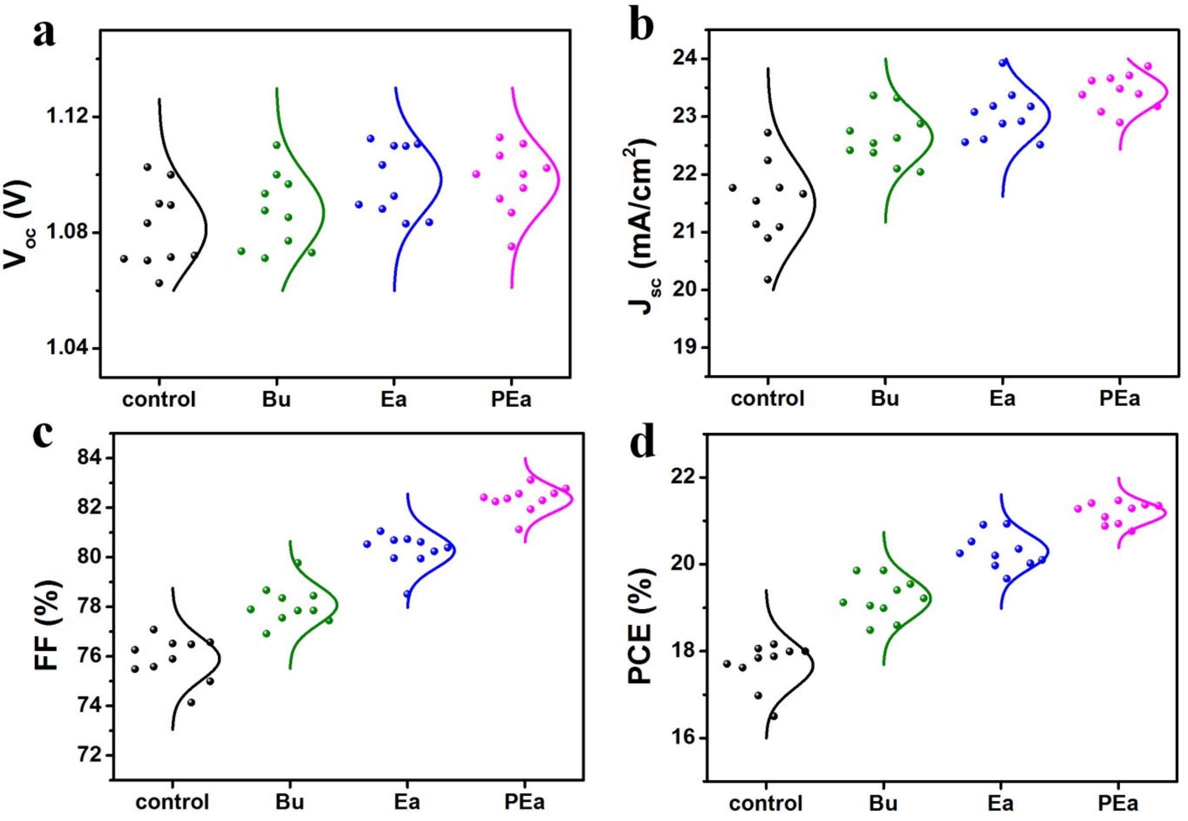

Fig. S21 Photovoltaic parameters statistics distribution of (a) J_{sc}, (b) V_{oc}, (c) *FF* and (d) PCE for the devices prepared from the four different perovskite films. (10 devices were collected from the different batch).

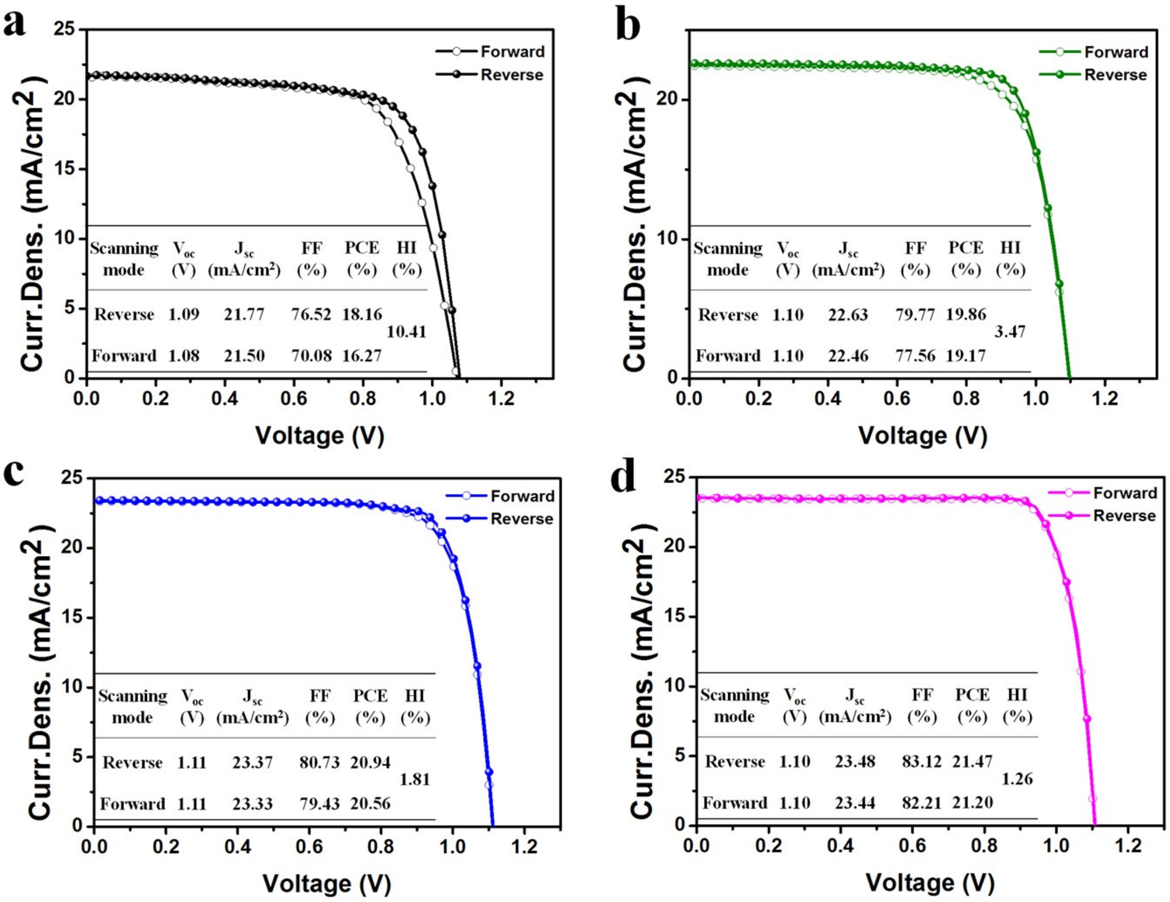

(a)

Scanning mode	V_{oc} (V)	J_{sc} (mA/cm²)	FF (%)	PCE (%)	HI (%)
Reverse	1.09	21.77	76.52	18.16	10.41
Forward	1.08	21.50	70.08	16.27	

(b)

Scanning mode	V_{oc} (V)	J_{sc} (mA/cm²)	FF (%)	PCE (%)	HI (%)
Reverse	1.10	22.63	79.77	19.86	3.47
Forward	1.10	22.46	77.56	19.17	

(c)

Scanning mode	V_{oc} (V)	J_{sc} (mA/cm²)	FF (%)	PCE (%)	HI (%)
Reverse	1.11	23.37	80.73	20.94	1.81
Forward	1.11	23.33	79.43	20.56	

(d)

Scanning mode	V_{oc} (V)	J_{sc} (mA/cm²)	FF (%)	PCE (%)	HI (%)
Reverse	1.10	23.48	83.12	21.47	1.26
Forward	1.10	23.44	82.21	21.20	

Fig. S22 *J*–*V* characteristics of the (a) control, (b) Bu-, (c) Ea- and (d) PEa-modified PSCs under both the reverse and forward scan directions. The HI in inset table represents the hysteresis index of device.

The corresponding hysteresis index of these devices was calculated according to a formula: hysteresis index = $((PCE_{reverse}-PCE_{forward})/ PCE_{reverse})*100$. An inconspicuous hysteresis loop is observed from these optimized devices, especially the PEa-modified device exhibits hysteresis-free behavior compared with the control device, which is likely due to the high quality of perovskite film as well as the reduced defects and excellent carrier transport at both anode and cathode sides.[5]

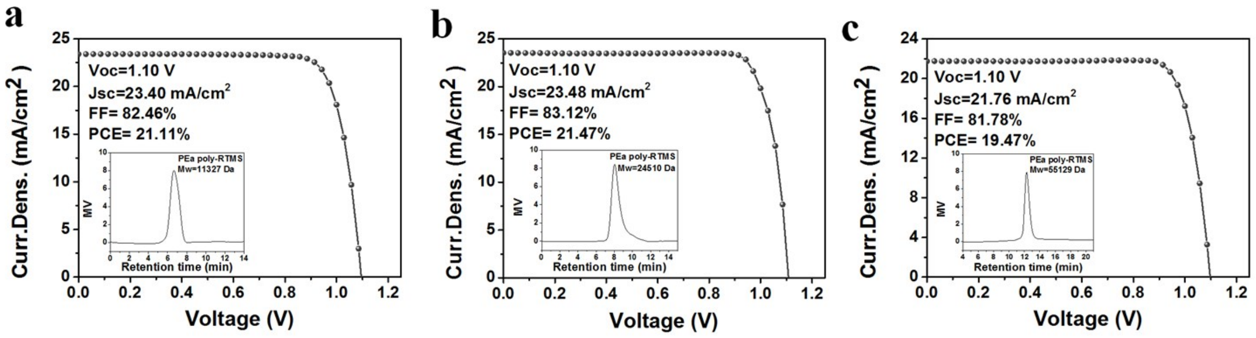

Fig. S23 *J*-*V* characteristic of PSCs modified by PEa poly-RTMS with different relative molecular weights.

We have synthesized another two PEa poly-RTMS with different relative molecular weights (i.e., Mw=11327 Da and Mw=55129 Da) by adjusting the reaction time between Ea monomer and AIBN initiator (i.e., Mw=11327 Da, 8 hours; Mw=24510 Da, 12 hours; Mw=55129 Da, 30 hours). Then, we investigate the effect of molecular weight on the device performance. As shown in Fig. S23, the devices modified by PEa poly-RTMS with different molecular weights show higher efficiency than that of control device. Among the PEa poly-RTMS modified devices, the PCE of device modified by PEa poly-RTMS with a relatively low molecular weight (Mw=11327 Da) is 21.11%. By contrast, the PCE of device modified by PEa poly-RTMS with a high molecular weight (Mw=55129 Da) decline to 19.47%. The PEa poly-RTMS is an ionic polymer, and a large relative molecular weight could cause the loss of its own conductivity, which lead to sub-optimal efficiency of device.

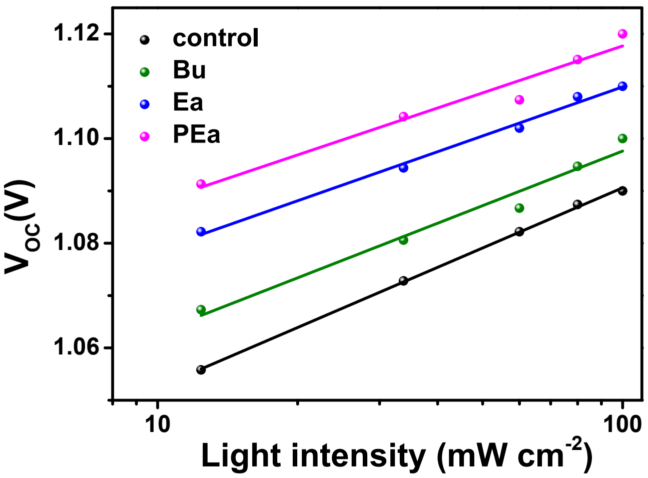

Fig. S24 Dependence of V_{OC} on light intensity of the control, Bu-, Ea- and PEa-modified devices.

The dependence of V_{oc} characteristic on the light intensity were performed to reveal more information on the recombination mechanisms. The relationship between V_{oc} and light intensity (*I*) is determined by $\sigma V_{oc} = KT/q$ for trap-free conditions.[1] The PEa-modified device possesses the smallest slope of 1.16KT/q than that of the control (1.48), Bu- (1.35), and Ea-modified device (1.21).

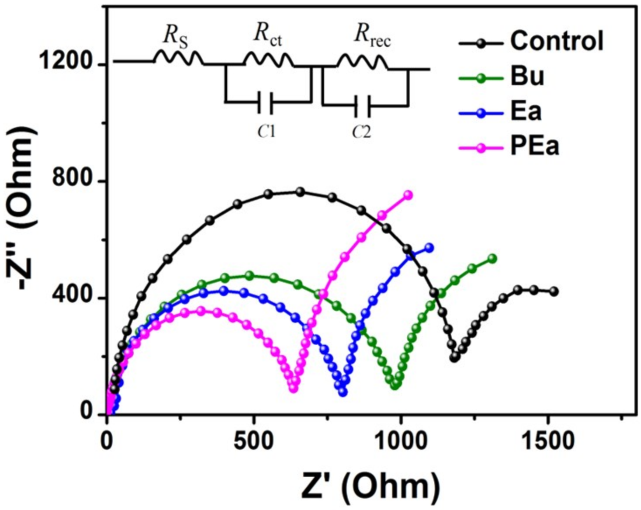

Fig. S25 Nyquist plots of four type of devices obtained at a bias of 0.8 V in the frequency ranging from 1 MHz to 0.1 Hz in the dark. Inset: the equivalent circuit model for fitting the plots.

As evidenced in Nyquist plots, the charge transport resistance (R_{ct}) and the recombination resistance (R_{rec}) corresponding to high-frequency and low-frequency are shown, respectively.[6] According to the equivalent circuit, the fitting R_{ct} (R_{rec}) are 1326 (899), 945 (1204), 771 (1438), and 662 (1870) Ω for control, Bu-, Ea-, and PEa-modified devices, respectively.

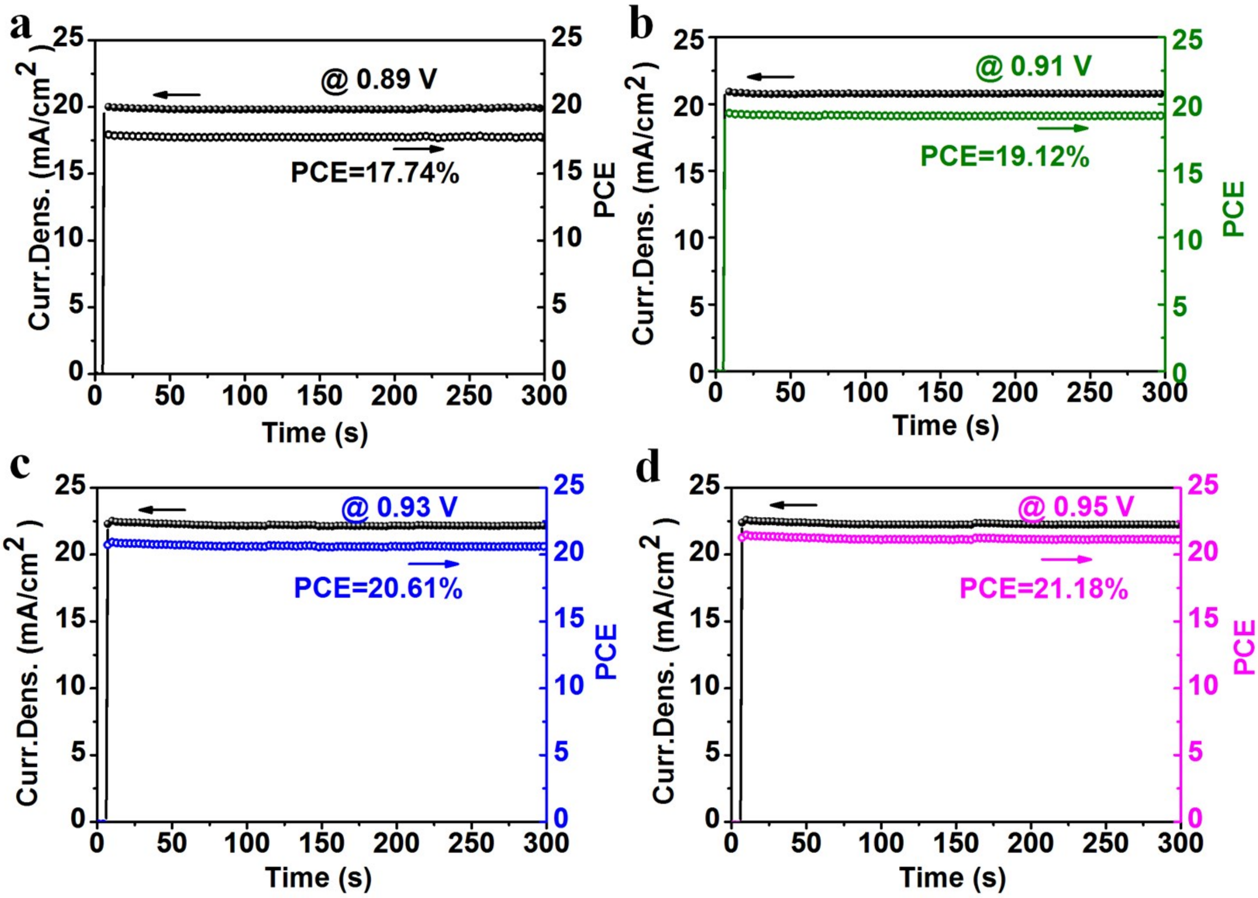

Fig. S26 Steady-state PCE measured under maximum power point tracking for 300 s of the (a) control, (b) Bu-, (c) Ea- and (d) PEa-modified PSCs.

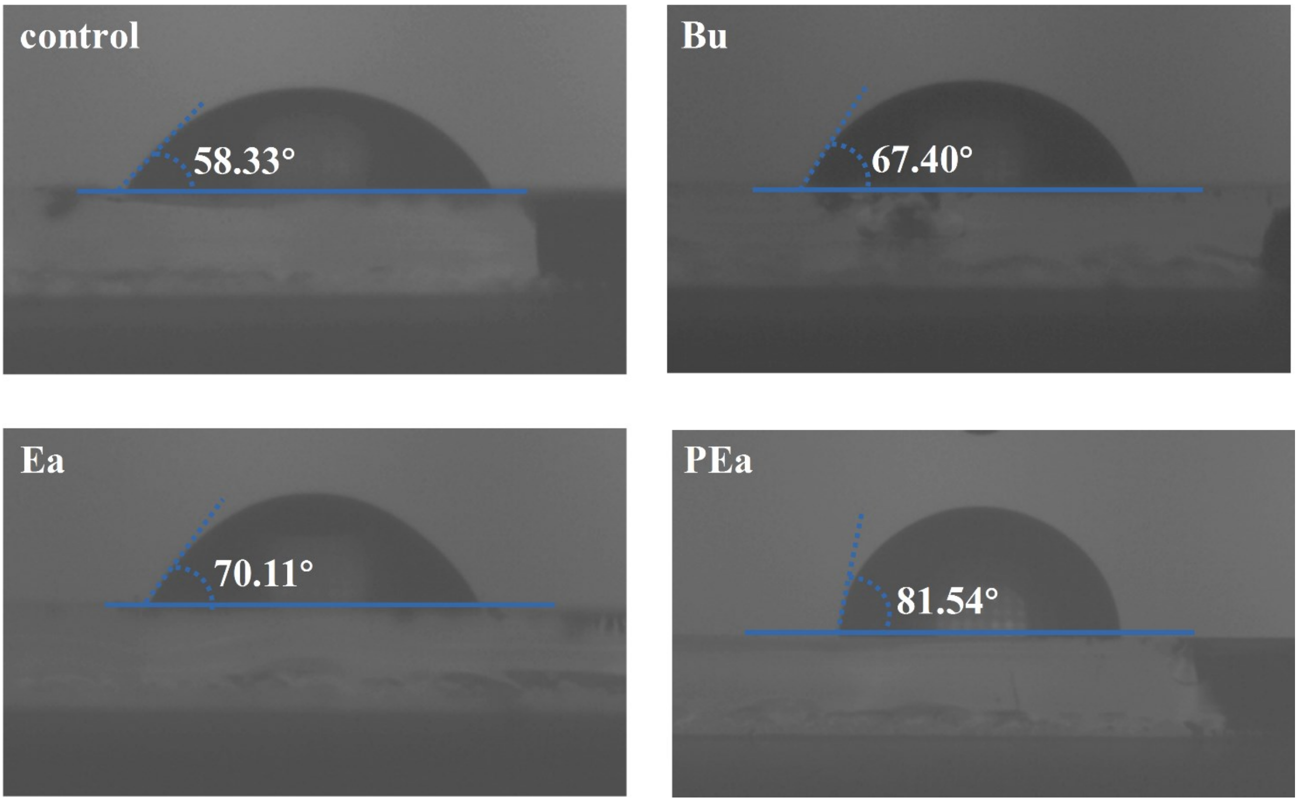

Fig. S27 Water contact angle measurements of the perovskite films based on the control, Bu, Ea and PEa.

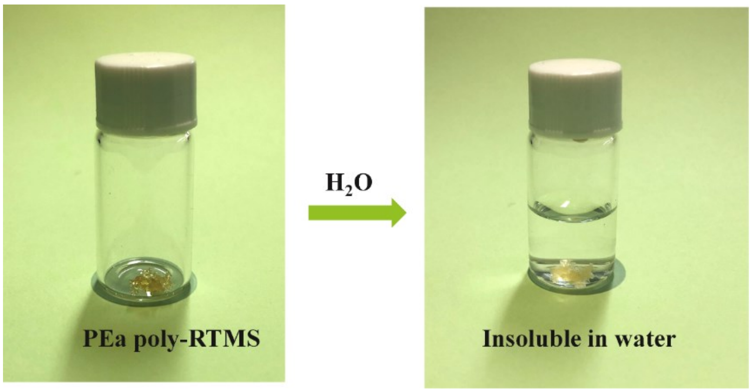

Fig. S28 Photographs of the PEa poly-RTMS dissolved in water.

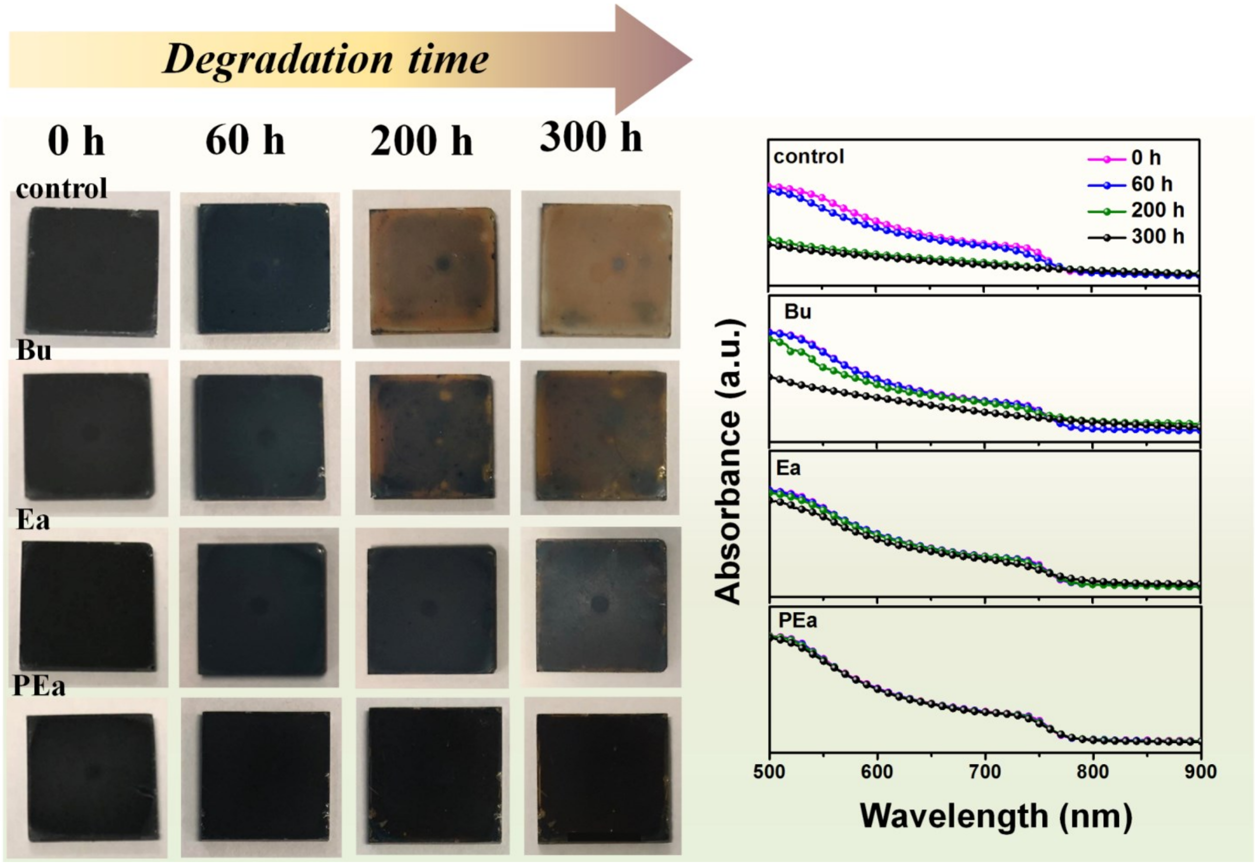

Fig. S29 (a) Photographs and (b) monitoring perovskite degradation of the control, Bu-, Ea- and PEa-modified films by UV-Vis absorption spectroscopy after thermal ageing at 85 ^{o}C for different times at RH= 40±5% in outdoor environment.

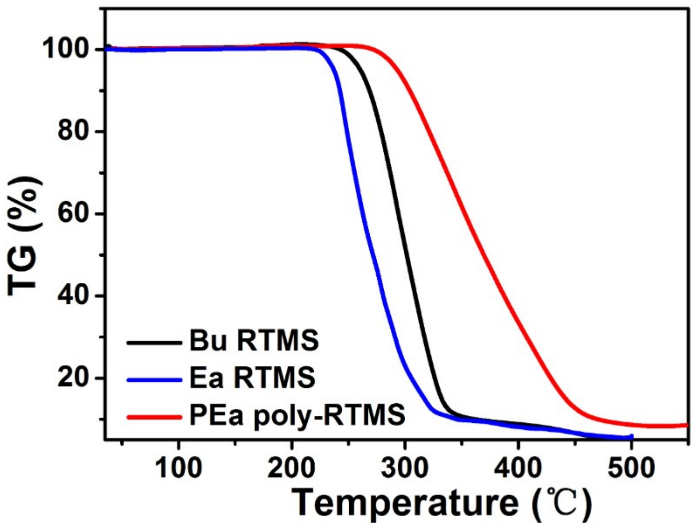

Fig. S30 Thermogravimetric analysis (TGA) of the Bu, Ea RTMS and PEa poly-RTMS.

The PEa poly-RTMS began to lose weight above 268 ^{o}C. When the test temperature increased to 347 ^{o}C, the thermal weight loss rate reached the maximum. The termination temperature of thermal decomposition is about 460 °C. The PEa poly-RTMS exhibits good thermal stability.

Table S1. Summary of device performance for Bu-modified PSCs based on different concentration. The devices were measured under 100 mW/cm^2 AM 1.5 G illumination.

m[a)]	Voc [V]	Jsc [mA/cm^2]	FF [%]	PCE [%]
0.05 mg/ml	1.09	22.37	76.72	18.79
0.10 mg/ml	1.10	22.51	77.96	19.30
0.30 mg/ml	1.10	22.63	78.77	19.61
1.20 mg/ml	1.10	21.87	77.75	18.78
control	1.09	21.77	76.52	18.16

a) represents the concentration of Bu RTMS relative to precursor solution.

Table S2. Summary of device performance for Ea-modified PSCs based on different concentration. The devices were measured under 100 mW/cm^2 AM 1.5 G illumination.

m[a)]	V_{oc} [V]	J_{sc} [mA/cm^2]	FF [%]	PCE [%]
0.10 mg/ml	1.09	22.26	78.79	19.06
0.30 mg/ml	1.10	22.36	78.86	19.40
0.60 mg/ml	1.11	23.37	80.73	20.94
0.80 mg/ml	1.08	22.83	78.57	19.37
control	1.09	21.77	76.52	18.16

a) represents the concentration of Ea RTMS relative to precursor solution.

Table S3. Summary of device performance for PEa-modified PSCs based on different concentration. The devices were measured under 100 mW/cm^2 AM 1.5 G illumination.

$m^{a)}$	V_{oc} [V]	J_{sc} [mA/cm^2]	FF [%]	PCE [%]
0.003%	1.09	22.19	79.54	19.23
0.030%	1.10	22.63	80.60	20.15
0.130%	1.10	23.48	83.12	21.47
1.300%	1.10	23.30	82.14	21.06
control	1.09	21.77	76.52	18.16

a) represents the mass percentage of PEa poly-RTMS relative to mass of precursor $PbBr_2$.

Table S4. Literatures summary of perovskite solar cells with RTMS modifiers.

Device structure	Interface (I)/bulk (B)	Molecular Structure	PCE [%]	Stability test results	Test conditions for stability
FTO/SnO_2/$FA_{0.75}MA_{0.25}PbI_{2.5}Br_{0.5}$/Spiro/Au[7]	I	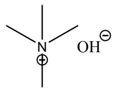	20.28%	97% PCE after 360 h	encapsulated devices, desiccator, RH=15%
FTO/NiO_x/$MAPbI_3$/PCBM/Ag[8]	I	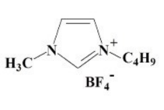	19.3%	a. 50% PCE after 190 h b. 73% PCE after 95 h	a. N_2 atmosphere, room temperature b. N_2 atmosphere, 80 °C
FTO/SnO_2/$FA_{0.83}MA_{0.17}Pb(I_{0.83}Br_{0.17})_3$ /Spiro/Au[9]	I	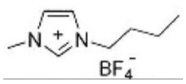	20.8%	none	-
FTO/Nb_2O_5/PCBM/$MAPbI_xCl_{3-x}$/Spiro/Au[10]	I		18.8%	none	-
FTO/C_{60}/$MAPbBr_3$/Spiro/Au[11]	I	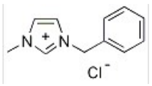	5.88%	65% PCE after 360 h	RH=20–30%, ambient, 25 °C
FTO/SnO_2/$FA_{0.95}MA_{0.05}PbI_{2.85}Br_{0.15}$/Spiro/Au[12]	I	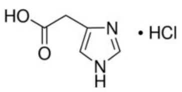	20.96%	94% PCE after 840 h	ambient, dark, room temperature
FTO/TiO_2/$MAPbI_3$/Spiro/Au[13]	I	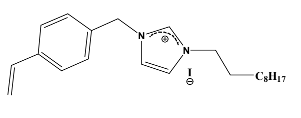	19.51	a. 80% PCE after 700 h b. 83% PCE after 700 h	a. unencapsualted, ambient, RH=40 ± 5%, room temperature b. unencapsulated, 60 °C, MPP, Ar, continuous light illumination
FTO/TiO_2/$(FAPbI_3)_{0.85}(MAPbBr_3)_{0.15}$/Spiro/Au[14]	B	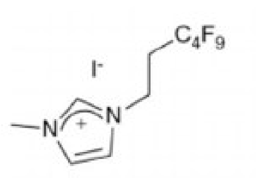	15.38	slight increase PCE after 1248 h	unencapsulated, RH= 57–60%, ambient, dark

(*continued on next page*)

FTO/NiO_x/$MAPbI_3$ /PCBM/Ag[15]	B	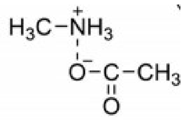	19.58%	a. 90% PCE after 1000 h b. 80% PCE after 500 h	a. AM 1.5 irradiance b. dark, 85 °C, RH<20%
FTO/TiO_2/$MAPbI_3$/ Spiro/Au[16]	B	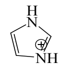	19.44	70% PCE after 300 h	illumination, MPP, inert environment, unencapsulated device, 60 °C
ITO/TiO_2/ $C_7H_{16}N_3PbI_3PF_6$/ CuSeCN/Au[17]	B	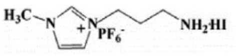	17.3%	98% PCE after 960 h	RH=57%
FTO/SnO_2/ $MAPbI_3$/Spiro/ Au[18]	B	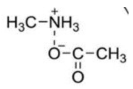	17.07%	none	
FTO/ZnO/$MAPbI_3$/ Spiro/Au[19]	B	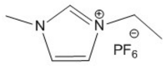	13.5%	93.5% PCE after 1080 h	ambient, RH=35%
FTO/TiO_2/$MAPbI_3$/ Spiro/Au[20]	B	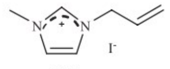 CC2 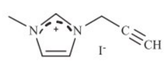 CC3 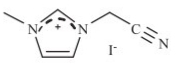 CN	CC2: 19.21% CC3: 18.38% CN: 16.34%	CC2 devices maintained 55% PCE after 480 h	illumination, MPP, Ar atmosphere
FTO/TiO_2/ $(Cs_{0.05}(MA_{0.15}FA_{0.85})_{0.95}Pb(I_{0.85}Br_{0.15})_3$ Spiro/Au[21]	B	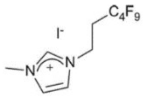	16.32%	90% PCE for >3600h	ambient, RH=55–60%
FTO/TiO_2/$MAPb_3$/ Spiro/Au[22]	B	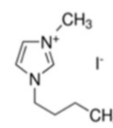	15.6%	none	-
FTO/TiO_2/$MAPb_3$/ Spiro/Au[23]	B	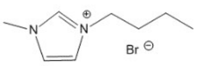	10.55%	85% PCE after 20 min	85 °C, RH=50%

(*continued on next page*)

FTO/TiO_2/ $MAPbI_3$/carbon[24]	B	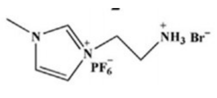	13.01%	94% PCE after 840 h	dark, RH=20%, 25 °C, illumination
ITO/CPTA/BACl/$FA_{0.9}Cs_{0.1}PbI_3$/Spiro/ MoO3/Au[25]	B	$CH_3NH_3CH_3COO$	20.05% (fabricated in ambient air)	a. 93% PCE after 1000 h b. 80% PCE after 700 h	a. unencapsulated device, air b. light, glove box
FTO/NiO_x/ $(FA_{0.83}MA_{0.17})_{0.95}Cs_{0.05}Pb(I_{0.9}Br_{0.1})_3$/ PCBM/BCP /Cr/Au[26]	B	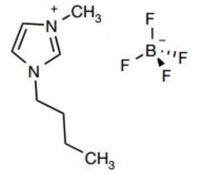	19.8%	95% PCE after1885 h	ambient, illumination, 70–75 °C
ITO/TiO_2/$MAPbI_3$/ Spiro/Au[27] Our previous work	B	MA/EATZ 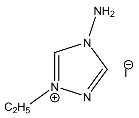 MA/BATZ 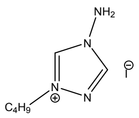 MA/OATZ 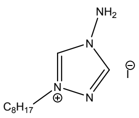	MA/EATZ : 20.03% MA/BATZ : 18.72% MA/OATZ : 17.33%	80% PCE for MA/OATZ, 75% PCE for MA/BATZ, 68% PCE for MA/EATZ, after 3500 h	RH=40±5%, room temperature
Our present work	B	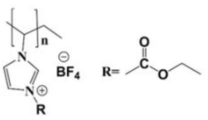	21.47%	over 92% PCE after 1200 h	ambient, illumination, 70-75 °C

References

1. W. Huang, S. Sadhu and S. Ptasinska, *Chem. Mater*. 2017, **29**, 8478.
2. A. Choukourov, H. Biederman, I. Kholodkov, D. Slavinska, M. Trchova and A. Hollander, *J. Appl. Polym. Sci.* 2004, **92**, 979.
3. T. Singh and T. Miyasaka, *Adv. Energy Mater.*, 2018, **8**, 1700677.
4. R. Azmi, N. Nurrosyid, S.-H. Lee, M. Al Mubarok, W. Lee, S. Hwang, W. Yin, T. K. Ahn, T.-W. Kim, D. Y. Ryu, Y. R. Do and S.-Y. Jang, *ACS Energy Lett.*, 2020, **5**, 1396-1403.
5. M. M. Tavakoli, P. Yadav, D. Prochowicz, M. Sponseller, A. Osherov, V. Bulović and J. Kong, *Adv. Energy Mater.*, 2019, **9**, 1803587.
6. P. Liu, W. Wang, S. Liu, H. Yang and Z. Shao, *Adv. Energy Mater.*, 2019, **9**, 1803017.
7. C. Huang, P. Lin, N. Fu, K. Sun, M. Ye, C. Liu, X. Zhou, L. Shu, X. Hao, B. Xu, X. Zeng, Y. Wang and S. Ke, *J. Mater. Chem. A*, 2018, **6**, 22086-22095.
8. M. Li, C. Zhao, Z.-K. Wang, C.-C. Zhang, H. K. H. Lee, A. Pockett, J. Barbé, W. C. Tsoi, Y.-G. Yang, M. J. Carnie, X.-Y. Gao, W.-X. Yang, J. R. Durrant, L.-S. Liao and S. M. Jain, *Adv. Energy Mater.*, 2018, **8**, 1801509.
9. N. K. Noel, S. N. Habisreutinger, B. Wenger, Y. H. Lin, F. Zhang, J. B. Patel, A. Kahn, M. B. Johnston and H. J. Snaith, *Adv. Energy Mater.*, 2019, **10**, 1903231.
10. Y. Guo, J. Tao, F. Shi, X. Hu, Z. Hu, K. Zhang, W. Cheng, S. Zuo, J. Jiang and J. Chu, *ACS Appl. Energy Mater.*, 2018, **1**, 2000-2006.
11. J. Luan, J. Xu, J. Chen, X. Shi, B. Zhang, S. Dai and J. Yao, *J. Solid State Chem.*, 2019, **270**, 436-442.
12. J. Chen, X. Zhao, S.-G. Kim and N.-G. Park, *Adv. Mater.*, 2019, **31**, 1902902.
13. R. Xia, Z. Fei, N. Drigo, F. D. Bobbink, Z. Huang, R. Jasiūnas, M. Franckevičius, V. Gulbinas, M. Mensi, X. Fang, C. Roldán ‐ Carmona, M. K. Nazeeruddin and P. J. Dyson, *Adv. Funct. Mater.*, 2019, **29**, 1902021.
14. M. Salado, F. J. Ramos, V. M. Manzanares, P. Gao, M. K. Nazeeruddin, P. J. Dyson and S. Ahmad, *ChemSusChem*, 2016, **9**, 2708-2714.
15. Y. Wu, F. Xie, H. Chen, X. Yang, H. Su, M. Cai, Z. Zhou, T. Noda and L. Han, *Adv. Mater.*, 2017, **29**, 1701073.
16. M. Salado, A. D. Jodlowski, C. Roldan-Carmona, G. de Miguel, S. Kazim, M. K. Nazeeruddin and S. Ahmad, *Nano Energy*, 2018, **50**, 220-228.
17. J. Wang, X. Ye, Y. Wang, Z. Wang, W. Wong and C. Li, *Electrochim. Acta*, 2019, **303**, 133-139.
18. Y. Xiao, L. Yang, G. Han, Y. Li, M. Li and H. Li, *Org. Electron.*, 2019, **65**, 201-206.
19. W. Zhang, Z. Ren, Y. Guo, X. He and X. Li, *Electrochim. Acta*, 2018, **268**, 539-545.
20. Y. Zhang, Z. Fei, P. Gao, Y. Lee, F. F. Tirani, R. Scopelliti, Y. Feng, P. J. Dyson and M. K. Nazeeruddin, *Adv. Mater.*, 2017, **29**, 1702157.
21. M. Salado, M. A. Fernandez, J. P. Holgado, S. Kazim, M. K. Nazeeruddin, P. J. Dyson and S. Ahmad, *ChemSusChem*, 2017, **10**, 3846.
22. P. Chen, Y. Zhang, J.s Du, Y. Wang, X. Zhang and Y. Liu, *J. Phys. Chem. C*, 2018, **122**, 10699-10705.
23. J. Du, Y. Wang, Y. Zhang, G. Zhao, Y. Jia, X. Zhang and Y. Liu, *Phys. Status Solidi RRL*, 2018, **12**, 1800130.
24. X. Zhou, Y. Wang, C. Li and T. Wu, *Chem. Eng. J.*, 2019, **372**, 46-52.
25. L. Chao, Y. Xia, B. Li, G. Xing, Y. Chen and W. Huang, *Chem*, 2019, **5**, 1-12.
26. S. Bai, P. Da, C. Li, Z. Wang, Z. Yuan, F. Fu, M. Kawecki, X. Liu, N. Sakai, J. T. Wang, S. Huettner, S. Buecheler, M. Fahlman, F. Gao and H. J. Snaith, *Nature*, 2019, **571**, 245-250.
27. S. Wang, Z. Li, Y. Zhang, X. Liu, J. Han, X. Li, Z. Liu, S. Liu and W. C. H. Choy, *Adv. Funct. Mater.*, 2019, **29**, 1900417.